Contactless Energy Transfer for Office and Domestic Applications

Contactless Energy Transfer for Office and Domestic Applications.

C. L. W. Sonntag, E. A. Lomonova, J. L. Duarte, A. J. A. Vandenput, and A. J. M. Pemen

***Abstract*— This paper presents a new method for shaping the magnetic field produced by multiple contactless energy transfer coils. It is shown in this work that by changing individual current phases of excited primary coils the shape of the magnetic field around the coils is changed. Furthermore, by carefully choosing specific coil current phases, the individual magnetic fields will cancel each other out far away from the coils but still retain most of their energy close to the coils. This is very beneficial when working with contactless energy transfer systems and electromagnetic interference (EMI) issues. A methodology for synthesis of a general multiple-input-multiple-output (MIMO) contactless energy transfer system is also presented. Using the methods described, the energy transfer capability as well as the efficiency of a theoretical test setup excited with in-phase current sources as well as out-of-phase current sources are then tested and compared. The magnetic field intensity around the two setups is also calculated and compared.**

***Index Terms*—Air-cored transformers, contactless energy transfer, magnetic field shaping, planar transformers.**

I. Introduction

CONTACTLESS energy transfer is the process in which electrical energy is transferred between primary and secondary coils through inductive coupling, without electrical contact between the coils. The transfer of energy between devices without the use of physical plugs is a fascinating concept to say the least. The potential applications for such a technology are practically endless and can range from the transfer of energy between low power home and office devices to high powered industrial applications. Medical, marine, and other applications where physical electrical contact might be dangerous, impossible or at the very least problematic, are all prospective candidates for the use of contactless energy transfer.

Currently many technical papers exist, where engineers and scientists have studied and researched different ways of transferring energy through an air gap [1], [6]. Almost none of these reports mention anything about shielding or regulations regarding magnetic field strengths, EMI, or human safety issues. Depending upon the amount of energy to be transferred in the contactless energy transfer system, it is possible that without proper shielding, magnetic fields produced by the system could exceed the maximum allowed values set out by a country's regulations; making it illegal and/or dangerous to human safety.

In this paper, a new method of shaping magnetic fields by changing the current phases of individual primary coils is presented. By choosing specific current phase shifts, it is possible to shape the magnetic field, so that in areas outside the coils, the individual magnetic fields cancel each other out, while still retaining most of their energy in the areas near the coils. This concept is demonstrated by creating a multi-input-multi-output contactless energy transfer system model. Based on this model, the energy transfer capability and efficiency of the system by first exciting it with in-phase currents, and then by out-of-phase currents are calculated. For both cases the magnetic field intensity is calculated around the coils to demonstrate the magnetic field cancellation effect.

II. Magnetic Field Shaping

In contactless energy transfer, the main method of transferring energy between primary and secondary coils is through induction and magnetic fields. When primary and secondary coils are coupled through air and do not have a core to guide the magnetic field, the magnetic field spreads out through the air without any predominant path. Because of this, not all of the magnetic field produced by the primary coil is coupled with the secondary coil. The stray magnetic field does not contribute to the transfer of energy between the coils and is a waste of energy. It is possible that part of the stray magnetic field could undesirably couple with other electronic circuits in their vicinity. This is very dangerous, since large magnetic fields could induce extra currents into nearby circuits, causing malfunction or even damaging them. Another concern is the safety of humans and other living matter when exposed to these stray magnetic fields.

Magnetic field shaping attempts to mold the magnetic field to maximize the coupling between primary and secondary coils and at the same time minimize the stray magnetic field. This can be done in two ways. First, magnetic field shaping is

Manuscript received June 30, 2006. This work was supported in part by the Dutch Agency of Economic Affairs - SenterNovem under the IOP EMVT project. C. L. W. Sonntag, Dr. E. A. Lomonova, Dr. J. L. Duarte, Prof. A. J. A. Vandenput, and Dr. A. J. M. Pemen are with the Electrical Engineering Department at Eindhoven University of Technology. Den Dolech 2, Impulse 1.08. P. O. Box 513, 5600 MB, Eindhoven, The Netherlands. (email: C.Sonntag@tue.nl).

done by changing the geometric shape of the coils. The Biot-Savart law for the magnetic field intensity clearly demonstrates this:

$$H(\boldsymbol{r}) = \frac{1}{4\pi}\int_{v'} \frac{J(\boldsymbol{r}')\times i_{r'r}}{|\boldsymbol{r}-\boldsymbol{r}'|^2}\,dv'. \quad (1)$$

The vector ***r'*** points from the axis origin to the current source, and the vector ***r*** points from the axis origin to the observation point, where the magnetic field intensity is calculated. According to (1) the magnetic field intensity at an observation point is partly dependent on the distance between the source and the observation point, and also the direction of the current density volume element. By guiding the current through specially shaped wires or tracks it is therefore possible to form the magnetic field. It has been shown in [1] that planar coils shaped into spiral forms, concentrate the magnetic field into a triangular pattern above the centre of the primary coils. Secondary coils placed inside this focused area will couple more strongly with the primary coils to increase their coupling and energy transfer capability.

Secondly, the authors propose another method for shaping magnetic fields produced by air coupled coils, by controlling individual coil current phases. In a magneto-quasi-static environment the net magnetic field intensity produced from multiple excited coils is the superpositioning of the magnetic fields from the individual coils. The magnetic fields produced from coils excited by in-phase currents will constructively add together to give a resultant magnetic field at the observer point. However, by exciting the individual coils with out-of-phase currents the individual magnetic fields will not necessarily constructively add together, and the resultant magnetic field at the observation point will be different than in the case of the in-phase currents. Using this method, the magnetic field shape of the coils can be modified without physically changing the coil geometry.

This idea can further be extended by realizing that magnetic fields are vectors, and that under certain conditions vectors can sum up to give a net effect of zero. For *N* vectors with constant modulus $|\boldsymbol{A}|$ adding together, they will each need a $2\pi/N$ phase shift from each other to have a zero net effect:

$$\sum_{n=0}^{N-1} |\boldsymbol{A}| \angle \frac{2\pi}{N} n = 0. \quad (2)$$

Although magnetic field intensities are strongly dependent on their distance from the source, it is possible to combine the above mentioned idea and the Biot-Savart law for calculating magnetic field intensities. By exciting a number of closely located coils, with the correct current phase shifts, the net magnetic field intensity at observer positions located relatively far from the sources will strive to zero.

This idea is demonstrated by using Ampere's law in integral form:

$$\oint_C \boldsymbol{H}\cdot d\mathrm{l} = \iint_S \boldsymbol{J}\cdot d\boldsymbol{A}, \quad (3)$$

to calculate the magnetic field intensities produced from three long thin parallel conductors, as shown in Fig. 1.

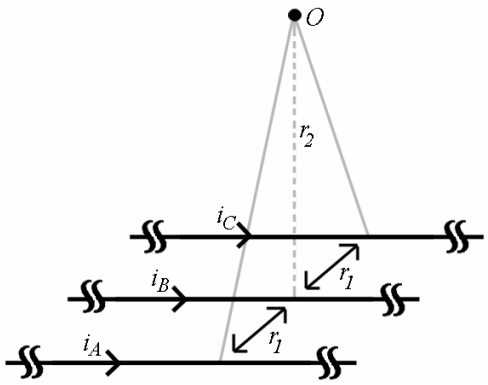

Fig. 1. Three long thin parallel conductors, each carrying a different current and spaced r_1 from one another.

Solving Ampere's law for the three conductors, the amplitude of the magnetic field intensity at observer position *O*, is given as:

$$H_O(t) = \frac{i_A(t)}{2\pi\sqrt{r_1^2+r_2^2}} + \frac{i_B(t)}{2\pi r_2} + \frac{i_C(t)}{2\pi\sqrt{r_1^2+r_2^2}}. \quad (4)$$

The three conductors are excited with cosine currents of the same amplitude I_0. Equation (2) is used to calculate their respective phases. Replacing the new source current values into (4) yields:

$$H_O(t) = \frac{I_0}{2\pi}\left(\frac{\cos(\omega t)}{\sqrt{r_1^2+r_2^2}} + \frac{\cos(\omega t+\frac{2\pi}{3})}{r_2} + \frac{\cos(\omega t-\frac{2\pi}{3})}{\sqrt{r_1^2+r_2^2}}\right). \quad (5)$$

By evaluating the magnetic field intensity relatively far from the three conductors $(r_2 >> r_1)$, the magnetic field intensity at time *t*=0 can be approximated by:

$$H_O(t=0) \approx 0. \quad (6)$$

In comparison, the magnetic field intensity, evaluated far from the three conductors but with in-phase current sources, is approximated by:

$$H_O(t=0) \approx \frac{3I_0}{2\pi r_2}. \quad (7)$$

There is a clear difference between (6) and (7) which confirms the cancellation effect of the magnetic field intensities due to the phase shifted current sources. The same cancellation of the magnetic field intensities at positions far from the source can be seen in coils and spirals excited with different phases, as will be demonstrated later in this paper.

III. Contactless Energy Transfer System Model

To illustrate the cancellation effect of the magnetic field intensities due to the phase shifted current sources, a model for a MIMO contactless energy transfer system is created. The multi-port transformer model is the model used to represent the contactless energy transfer system with its losses, as a whole. It can be used for systems with multiple primary sources as well as multiple secondary loads. The amount of primary circuits is given as *P*, and the amount of secondary circuits as *Q*. Fig. 2 shows a graphical representation of the model, where R_1 and L_1 are the lumped coil parameters, C_1 is the resonance capacitor and V_1 the voltage source for the first primary circuit. Similarly, Z_{L1} is the load impedance of the first secondary circuit. The mutual inductances between the coils are labeled *M*, with their appropriate numbers as subscripts.

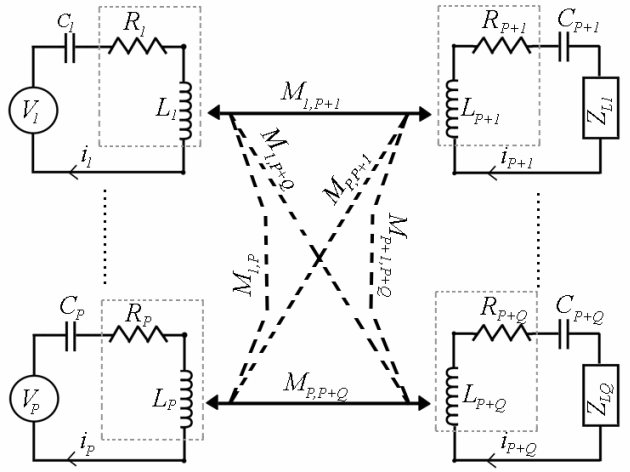

Fig. 2. A representation of the multi-port transformer model. Primary circuits and coils are on the left, secondary circuits and coils are on the right.

Energy transfer capabilities and efficiencies are strongly related to the electrical properties of the coils used in the contactless energy transfer system. These coils need to be modeled as accurately as possible. By driving the primary circuits with relatively low signal frequencies, the system can be assumed to be magneto-quasi-static, which greatly reduces the complexity of the circuits.

A. The coil lumped parameter model

At relatively low operating frequencies, the standard models for electrical components and circuits accurately describe their operating principle. However, at high frequencies when the propagation of electromagnetic fields becomes comparable to the signal period, these models no longer accurately predict the electrical circuit behavior, due to electromagnetic effects. In this paper the circuits are excited with relatively low frequency signals, typically up to 200 kHz, thus labeling the system magneto-quasi-static. This means that all dynamic solutions are comparable to the static ones and that standard electrical circuit models can be used. With this in mind the coils are modeled.

Proposed in [2] and [5] is the lumped inductor model for coils placed on a substrate, like planar PCB coils and spirals. The lumped model is made up of two main parts: the series inductance, resistance and capacitance of the coils and a parallel capacitance and resistance which combine the effects of the substrate losses. The substrate losses are frequency dependent [5] and neglected in our model. Due to the geometric shape of inductors, their series capacitance is also negligible [7] (typically, in the order of a few picofarad) and much smaller than the externally added resonance capacitor, which is explained in a later subsection. The inductor model for the coils becomes a resistor in series with an inductor.

Extracting the lumped parameters from the coils is mainly done in Maxwell 3D version 11 (Ansoft Corporation). The coils are modeled in a 3D environment and simulated to solve the electromagnetic fields which in turn produce the lumped elements and parameters used in modeling the contactless energy transfer system.

The resistance of a coil is accurately estimated in Maxwell 3D by simulating it while using the eddy current solution type. By setting the adaptive frequency value, the solver incorporates high frequency- and proximity losses. The resistance of the coil is given as an output.

The series inductance of a coil is calculated by the amount of magnetic flux linkage it produces for a given electric current. The inductance of a coil can be estimated in Maxwell 3D by simulating it while using the magneto-static solution type.

The mutual inductance between coils represents the method through which magnetic energy is transferred between coils. The mutual inductance between all coils must be calculated. This can be done in the same fashion as the self inductance, except that the magnetic flux linkage produced by the primary coil, is evaluated through the surface of the secondary coil. The mutual inductance between coils can be estimated in Maxwell 3D by simulating two or more coils together, while using the magneto-static solution type.

To minimize losses in the primary and secondary circuits, the contactless energy transfer system runs in resonant mode. By adding a series capacitor to each coil it is possible to compensate the effect of the inductive reactance.

B. Primary and secondary circuit equations

To solve the primary and secondary circuit currents, all the circuit equations must be set up. The individual circuit

equations for the primary circuits are written in the form:

$$v_p = R_p i_p + u_{Cp} + \sum_{k=1}^{P+Q}\left[M_{pk} \frac{d}{dt} i_p \right], \tag{8}$$

$$i_p = C_p \frac{d}{dt} u_{Cp}, \tag{9}$$

$$\text{where } (1 \le p \le P),$$

and for the secondary circuits:

$$0 = Z_{Lq} i_q + R_q i_q + u_{Cq} + \sum_{k=1}^{P+Q}\left[M_{qk} \frac{d}{dt} i_q \right], \tag{10}$$

$$i_q = C_q \frac{d}{dt} u_{Cq}, \tag{11}$$

$$\text{where } (1 \le q \le Q), \text{ see Fig. 2.}$$

This results in a set of $2(P+Q)$ differential equations.

C. Solving the differential equations

The differential equations are solved by converting them into matrix representations and then manipulating those matrices into a state-space representation. Using Simulink (The MathWorks, Inc.) it is then possible to solve the circuit equations for a number of different inputs and outputs. The time-domain method utilizes a standard state-space representation of the system model, given by:

$$\dot{\boldsymbol{x}}(t) = \boldsymbol{A}\boldsymbol{x}(t) + \boldsymbol{B}\boldsymbol{u}(t), \tag{11}$$

$$\boldsymbol{y}(t) = \boldsymbol{C}\boldsymbol{x}(t) + \boldsymbol{D}\boldsymbol{u}(t). \tag{12}$$

In order to convert the circuit equations into the state-space format, all of the $2(P+Q)$ differential equations are written in a matrix representation as:

$$\left[\begin{array}{c|c} \boldsymbol{I} & \boldsymbol{0} \\ \hline \boldsymbol{0} & \boldsymbol{0} \end{array}\right]\left[\begin{array}{c} \boldsymbol{V} \\ \hline \boldsymbol{0} \end{array}\right] = \left[\begin{array}{c|c} \boldsymbol{M} & \boldsymbol{0} \\ \hline \boldsymbol{0} & \boldsymbol{C} \end{array}\right]\frac{d}{dt}\left[\begin{array}{c} \boldsymbol{i} \\ \hline \boldsymbol{U} \end{array}\right] + \left[\begin{array}{c|c} \boldsymbol{R} & \boldsymbol{I} \\ \hline -\boldsymbol{I} & \boldsymbol{0} \end{array}\right]\left[\begin{array}{c} \boldsymbol{i} \\ \hline \boldsymbol{U} \end{array}\right], \tag{13}$$

where the ***I***-matrix represents the identity matrix. The ***V***-matrix contains the input values, in this case the primary input voltages:

$$\boldsymbol{V} = \begin{bmatrix} V_1 & \cdots & V_P \end{bmatrix}^T. \tag{14}$$

The ***M***-matrix contains all the self inductance and mutual inductance values for the primary and secondary coils. The ***C***-matrix contains the resonant capacitor values for the primary and secondary coils. The ***R***-matrix contains the resistor values as well as the load values. The ***i***-matrix contains the current vectors, and the ***U***-matrix contains the capacitor voltage vectors. The ***i***-matrix and the ***U***-matrix make up the state-space vector which is used by Simulink. Equation (13) is rewritten in a condensed matrix form as:

$$\boldsymbol{K}'\left[\begin{array}{c} \boldsymbol{V} \\ \hline \boldsymbol{0} \end{array}\right] = \boldsymbol{M}'\frac{d}{dt}\left[\begin{array}{c} \boldsymbol{i} \\ \hline \boldsymbol{U} \end{array}\right] + \boldsymbol{R}'\left[\begin{array}{c} \boldsymbol{i} \\ \hline \boldsymbol{U} \end{array}\right], \tag{15}$$

where $\boldsymbol{K}' = \left[\begin{array}{c|c} \boldsymbol{I} & \boldsymbol{0} \\ \hline \boldsymbol{0} & \boldsymbol{0} \end{array}\right]$, $\boldsymbol{M}' = \left[\begin{array}{c|c} \boldsymbol{M} & \boldsymbol{0} \\ \hline \boldsymbol{0} & \boldsymbol{C} \end{array}\right]$ and $\boldsymbol{R}' = \left[\begin{array}{c|c} \boldsymbol{R} & \boldsymbol{I} \\ \hline -\boldsymbol{I} & \boldsymbol{0} \end{array}\right]$.

Substituting the state-space variables into (13) results in:

$$\boldsymbol{K}'\boldsymbol{u} = \boldsymbol{M}'\dot{\boldsymbol{x}} + \boldsymbol{R}'\boldsymbol{x}. \tag{16}$$

Further manipulation of (16) yields:

$$\dot{\boldsymbol{x}} = \left(-\boldsymbol{M}'^{-1}\boldsymbol{R}'\right)\boldsymbol{x} + \left(\boldsymbol{M}'^{-1}\boldsymbol{K}'\right)\boldsymbol{u}. \tag{17}$$

Equation (17) is now formulated in state-space format and gives the state matrix, $\boldsymbol{A} = \left(-\boldsymbol{M}'^{-1}\boldsymbol{R}'\right)$ and $\boldsymbol{B} = \left(\boldsymbol{M}'^{-1}\boldsymbol{K}'\right)$. Similarly, the matrix equation which specifies the output of the system is:

$$\left[\begin{array}{c} \boldsymbol{i} \\ \hline \boldsymbol{U} \end{array}\right] = \left[\begin{array}{c|c} \boldsymbol{I} & \boldsymbol{0} \\ \hline \boldsymbol{0} & \boldsymbol{I} \end{array}\right]\left[\begin{array}{c} \boldsymbol{i} \\ \hline \boldsymbol{U} \end{array}\right] + \left[\begin{array}{c|c} \boldsymbol{0} & \boldsymbol{0} \\ \hline \boldsymbol{0} & \boldsymbol{0} \end{array}\right]\left[\begin{array}{c} \boldsymbol{V} \\ \hline \boldsymbol{0} \end{array}\right]. \tag{18}$$

Equation (18) is rewritten in a condensed matrix form as:

$$\left[\begin{array}{c} \boldsymbol{i} \\ \hline \boldsymbol{U} \end{array}\right] = \boldsymbol{C}\left[\begin{array}{c} \boldsymbol{i} \\ \hline \boldsymbol{U} \end{array}\right] + \boldsymbol{D}\left[\begin{array}{c} \boldsymbol{V} \\ \hline \boldsymbol{0} \end{array}\right]. \tag{19}$$

There is no feed-forward control between the input voltages and the output currents, so the ***D***-matrix is equal to zero. By choosing the ***C***-matrix as the identity matrix, the circuit currents and capacitor voltages are given as the outputs.

The differential equations are solved by building and simulating the state-space model in Simulink. Appropriate voltage source amplitudes and frequencies are given as inputs to the model, and after a successful model simulation, returns the individual circuit current waveforms. These waveforms are used to calculate power transfer values.

D. Calculating power transfer capabilities and efficiencies

Using the steady-state current values from the Simulink model output, the powers at the sources and loads are calculated. The apparent power drawn from the primary sources is given by:

$$S_p = (1/2)\left(V_p I_p\right), \text{ where } (1 \le p \le P), \tag{20}$$

and the apparent power delivered to the secondary loads as:

$$S_{P+q} = (1/2)\left(I_{P+q}^2 Z_{Lq}\right), \text{ where } (1 \le q \le Q). \quad (21)$$

The total apparent power from all the primary sources then becomes:

$$S_{Primary} = \sum_{p=1}^{P} S_p. \quad (22)$$

Similarly, the total apparent power delivered to the secondary loads is:

$$S_{Secondary} = \sum_{q=1}^{Q} S_{P+q}. \quad (23)$$

Finally, the apparent power transfer efficiency is given as:

$$E_{eff} = \frac{S_{Secondary}}{S_{Primary}} \cdot 100\%. \quad (24)$$

This value tells how efficient the system is at transferring the magnetic energy across the air gap. Using these results the power losses in the different components can be calculated as well as the influence of different input and output parameters.

IV. Theoretical Test and Results

The magnetic field cancellation effect is tested by theoretically simulating a contactless energy transfer system based on the methods described in this paper. In the first test the primary coils are exited using in-phase currents.

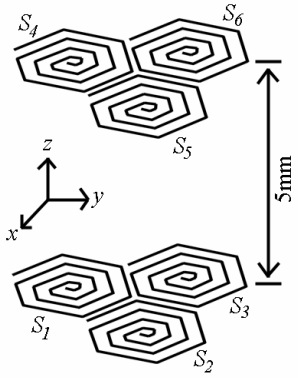

Fig. 3. A graphical representation of the test setup with the three primary coils S_1, S_2 and S_3 at the bottom, and the three secondary coils S_4, S_5 and S_6 at the top.

In the second test the primary coils are excited using out-of-phase currents to demonstrate the magnetic field cancellation effect. In both cases the power transfer capability and efficiency of the system as well as the magnetic field intensity at a few positions around the primary coils are calculated and finally compared. Purely resistive loads are used in these tests. The contactless energy transfer system used in these tests consists of three primary hexagon spiral coils and three secondary hexagon spiral coils, placed at exactly 5 mm above each other as shown in Fig. 3. All six hexagon spiral coils used in the contactless energy transfer system are identical, and their dimensions and electrical properties are given in Table I.

TABLE I
Dimensions and Electrical Properties of the Hexagon Spiral Coils.

Parameter	Value
Radius	48 mm
Track width	2.133 mm
Inter track spacing	0.8 mm
Copper thickness	0.1 mm
Inductance (L)	6.461 μH
Resistance (R)	21.34 μΩ
Resonant capacitance (C)	174.25 μF
Operating frequency (f)	150 kHz
Spiral coil turns (N)	14
Input voltages ($V_1 \ldots V_3$)	2.5 V

A. *In-phase simulation test*

Using the techniques described in this paper, all three primary coils $S_{1...}S3$ are excited with an in-phase current signal. The primary power and load power are calculated and shown in Fig. 4.

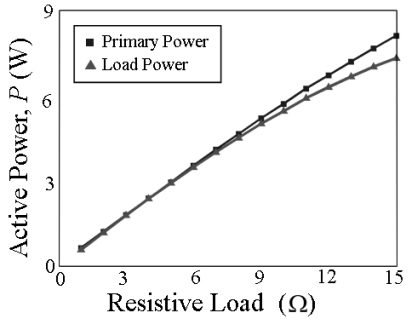

Fig. 4. The primary power and load power results from the in-phase test.

B. *Out-of-phase simulation test*

In the out-of-phase test the three primary coils are excited with 120 degree phase shifts. The primary power and load power are calculated and shown in Fig. 5.

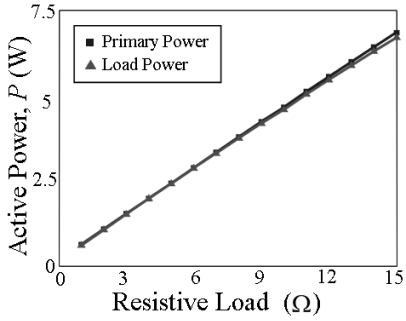

Fig. 5. The primary power and load power results from the out-of-phase test.

C. Simulation test results

Comparing Fig. 4, and Fig. 5, it is seen that the power transfer in the two tests is almost the same, although the out-of-phase test shows a lower power transfer for the same resistive load values. The power transfer efficiency for both tests is calculated and illustrated in Fig. 6.

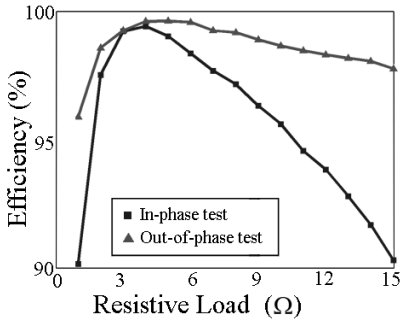

Fig. 6. The power transfer efficiency results from both tests.

Both tests show a very high power transfer efficiency with a maximum of about 99%. From these results we conclude that there is no major performance difference between these two tests (efficiency between 90% and 99%), but some improvement can be obtained in this particular range of resistive load values by using out-of-phase currents. Using a simplified solution for the Biot-Savart equation, called the current stick method [3], the absolute magnetic field intensities are calculated around the primary coils, during both tests. The six measuring points at a distance of 10 times the hexagon spiral coil radius (480 mm) are located in the three dimensions around the primary coils, as shown in Fig. 7. The data is tabulated and compared in Table II.

TABLE II
Calculated magnetic field intensity values

Measuring point	Absolute magnetic field intensity for the in-phase test	Absolute magnetic field intensity for the out-of-phase test	Ratio
O_1	120.8 (10^{-3}) A · m $^{-1}$	9.2 (10^{-3}) A · m $^{-1}$	13.1
O_2	120.8 (10^{-3}) A · m $^{-1}$	9.2 (10^{-3}) A · m $^{-1}$	13.1
O_3	64.6 (10^{-3}) A · m $^{-1}$	1.2 (10^{-3}) A · m $^{-1}$	53.8
O_4	64.6 (10^{-3}) A · m $^{-1}$	1.2 (10^{-3}) A · m $^{-1}$	53.8
O_5	64.8 (10^{-3}) A · m $^{-1}$	11 (10^{-3}) A · m $^{-1}$	5.9
O_6	64.3 (10^{-3}) A · m $^{-1}$	8.6 (10^{-3}) A · m $^{-1}$	7.5

From these results a strong reduction of the stray magnetic field intensity away from the coils is seen, with reduction ratios between 5.9 and 53.8.

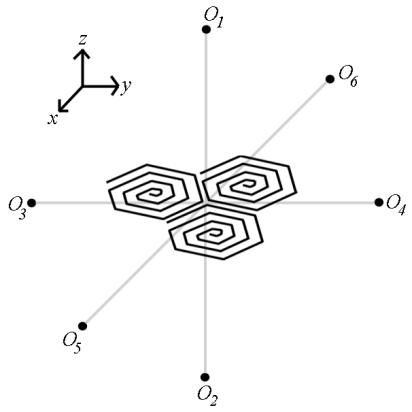

Fig. 7. The six magnetic field intensity measuring points, $O_1 \ldots O_6$ around the primary coils.

V. Conclusion

In this paper the authors proposed a new way of shaping a magnetic field produced from multiple primary coils, by exciting them with out-of-phase currents. A basic six coil contactless energy transfer system is simulated using a general MIMO contactless energy transfer model derived in this paper. After simulation of the system by in-phase and out-of-phase currents, the magnetic field intensities are calculated around the primary coils using the current stick method. The results show that, by exciting a multi-input contactless energy transfer system with dedicated out-of-phase currents, the stray magnetic fields are reduced without negatively affecting the power transfer capability or efficiency.

Acknowledgment

The authors would like to thank F. B. M. v. Horck as well as M. A. M. Hendrix for their valuable discussions regarding this work.

References

[1] S. Y. R. Hui, and Wing. W. C. Ho, "A New generation of Universal Contactless Battery Charging Platform for Portable Consumer Electronic Equiptment," IEEE Transactions on Power Electronics, Vol. 20, No. 3, pp. 620-627, May 2005.

[2] Sunderarajan S. Mohan, Maria Del Mar Hershenson, Stephen P. Boyd, and Thomas H. Lee, "Simple Accurate Expressions for Planar Spiral Inductances," IEEE Journal of Solid-State Circuits, Vol. 34, No. 10, pp. 1419-1424, October 1999.

[3] Herman A. Hous, and James R. Melcher, "Electromagnetic Fields and Energy," Massachusetts Institute of Technology, 1998, pp. 321-322.

[4] F. B. M. van Horch, "A Treatise on Magnetics & Power Electronics," Technische Universiteit Eindhoven, 2005, pp. 148-149.

[5] C. Patrick Yue, Changsup Ryu, Jack Lau, Thomas H. Lee, and S. Simon Wong, "A Physical Model for Planar Spiral Inductors on Silicon," Stanfort University, unpublished.

[6] R. Mecke, and C. Rathge, "High Frequency inverter for contactless energy transmission over large air gap," 35th Annual IEEE Power Electronics Specialists Conference, pp. 1737-1743, 2004.

[7] S. C. Tang, S. Y. Hui, and Henry Shu-Hung Chung, "Coreless Planar Printed-Circuit-Board (PCB) Transformers-A Fundamental Concept for Signal and Energy Transfer," IEEE Transactions on Power Electronics, Vol. 15, No. 5, pp. 931-941, September 2000.